International Journal of the JCRM
Japanese Committee for Rock Mechanics

Volume 4, Number 2, November 2009, pp 79-85
[ISSUE PAPER]

The effect of fabric-controlled layering on compressional and shear wave propagation in carbonate rock

Weiwei LI*, Christopher PETROVITCH**, Laura J. PYRAK-NOLTE ***

* *Member of ISRM: Department of Physics, Purdue University, West Lafayette, Indian 47907 USA*
** *Non-member of ISRM: Department of Physics, Purdue University, West Lafayette, Indian 47907 USA*
*** *Department of Earth and Atmospheric Sciences, Department of Physic, Purdue University, West Lafayette, Indian 47907 USA*

Received 18 10 2008; accepted 04 11 2009

ABSTRACT

Mixed chemical and clastic sedimentary processes form carbonate rock with fine bedding that results in a weakly directed fabric. Laboratory experiments were performed to determine the effect of fabric-controlled layering on compressional and shear wave propagation. X-ray tomographic scans of the sample found a density variation among the layers that ranged from 1700 kg/m^3 to 2300 kg/m^3 in a cubic sample 100 mm on edge. Wavefront imaging results show that the density contrasts among the layers produced energy confinement. The amplitude and arrival time of the compressional and shear waves are affected by saturation of the sample with water, i.e., by changing the impedance contrast among the layers. Seismic monitoring of the fluid-front during saturation indicates that the fine bedding also affects the hydraulic properties of the sample.

Keywords: Rock Mechanics, Carbonate, Seismic wave, Water Saturation, Fluid Front

1. INTRODUCTION

Carbonate rocks are geographically widespread, and often encountered in the construction of surface and subsurface infrastructure (e.g. tunnel and reservoir plan for Chicago, Illinois). Working in carbonate rocks is complex because the structural, chemical and physical properties of carbonate rock vary from site to site. This variation occurs because the physical properties of carbonate rock are strongly influenced by the rock fabric, which depends on the depositional environment as well as diagenetic and tectonic processes. The fabric of carbonate rock is often classified based on the major constituents (e.g., fossils, ooids, etc), pore space, fractures and styolites (Durrast & Siegesmund, 1999). The major constituents in the rock and the packing and cementation of these constituents result in heterogeneity in physical properties that span multiple length scales.

The most common form of heterogeneity is layering caused by a variation in porosity (Nurmi et al., 1990). The thickness of the layers can vary, and porosity within a layer may also vary. The variation in porosity among layers leads to anisotropic behavior in the hydraulic, mechanical and seismic properties of carbonate rocks.

The effect of thin layers on seismic wave propagation depends on the frequency content of the signal relative to the thickness of the layers as well as the impedance contrast between layers. For a broadband signal and a fixed layer thickness, selected frequencies are multiply reflected and result in amplitude and velocity dispersion (Schoenberg, 1974). In addition, the impedance contrast amongst layers can produce wave-guiding phenomena. Thus a wave transmitted through a layered medium is often subjected to competing scattering and attenuation mechanisms.

In this paper, we present the results of a laboratory study to examine the effect of fabric-controlled layering on seismic wave propagation through carbonate rock.

2. EXPERIMENTAL METHOD

2.1 Sample Preparation

Experiments were performed on cubic samples of Austin Chalk Cordova Cream obtained from Texas Quarries, Inc. The cubic samples were belt-sanded to remove surface roughness. Samples were labeled AC2 and AC5. AC5 was sealed with marine epoxy to enable water saturation. For AC5, three ports were attached to opposite sides of the cube as inlets (Side A) and outlets (Side C). AC2 was used for wavefront imaging experiment. The final dimension and properties of the samples are listed in Table 1. In addition, a cubic Aluminum sample with an edge length of 100 mm was used as a standard to calibrate the seismic array. A cubic Lucite (acrylic) sample with an edge length of 100 mm was used for system calibration for the wavefront imaging experiments.

From X-ray tomography, the density of these Austin

Chalk samples varied from 1700 kg/m^3 to 2300 kg/m^3 (Figure 1). From wet and dry gravimetric measurements, the porosity was found to range from 20% to 25%.

Table1. Dimensions, mass and density of samples

Sample	AC2	AC5
Dimensions (mm)		
A-C	100.5	99.7
B-D	99	101
E-F	101	99.7
Mass (g)	2176	2070
Density (kg/m^3)	2166	2056
Porosity		24%

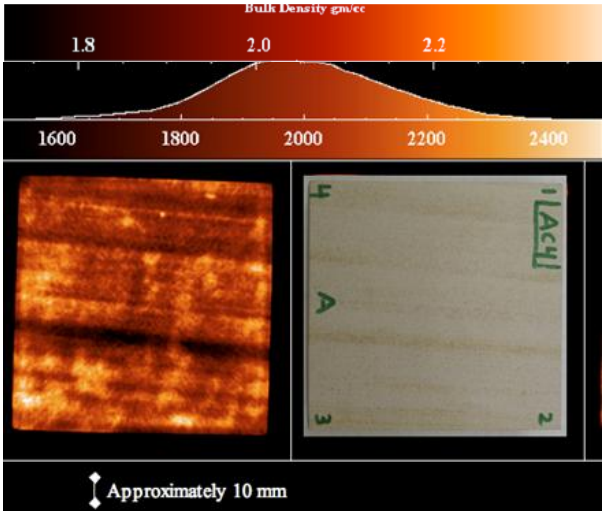

Figure1. On the lower left, X-ray tomographic scan of a cross section of a cubic sample of Austin Chalk measuring 100mm on edge. The upper color scale shown indicates the density of the sample in g/cc while the lower scale shows the distribution of CT numbers. On the lower right, a digital image of one end of the same sample shows weak layering in the rock and is oriented relative to the X-ray scan.

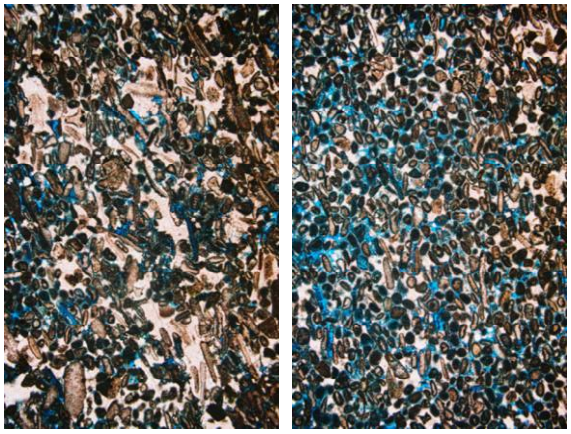

Figure 2. Two digital images from thin-sections of Austin Chalk. Blue areas represent pore spaces. Each image shows a 4.2 mm by 6.5 mm region of the rock. The left image is taken from a brown-colored layer and the image on the right is taken from a relatively white layer (see Figure 1 lower right).

A companion sample of Austin Chalk was thin-sectioned to determine the fabric of the rock. Figure 2 shows two digital images from the thin-sections. The petrographic report identified the rock as a bioclastic limestone with a mixed chemical and clastic sedimentary origin. Fine bedding defines a weakly directed fabric. The detrital framework grains (60%) are round and consist of 140-1000 μm calcite pellets (40%) plus calcite fossil fragments (20%). The contacts between grains are tangential. The cement between grains (40%) is composed of sparry calcite.

2.2 Seismic Method

Two experimental methods were used to characterize the seismic response of the carbonate samples: (1) wavefront imaging and (2) a seismic array. Wavefront imaging is used to determine the isotropy or anisotropy of a sample. The seismic array is used to characterize the compressional and shear wave response of a sample under stress or under other dynamic processes such as fluid invasion. These techniques are described below.

2.3 Wavefront Imaging

Wavefront imaging methods have been used to study the acoustic properties of crystalline solids (Wolfe, 1995), ocean and synthetic sediments (Mullenbach, 1996; Pyrak-Nolte et al., 1999) as well as fractures and fractured rock (Pyrak-Nolte et al., 1996; Xian et al., 2001; Oliger et al., 2003). In this technique, compressional-mode spherically focused, water-coupled piezoelectric transducers (central frequency 1.0 MHz) are used to send and receive the signal. The source transducer is maintained at the center of one side of the cubic sample while the receiver is translated over a 60mm by 60mm two-dimensional region to obtain the spatial distribution of energy with time. This technique results in a three-dimensional data set, i.e., two spatial dimensions and one temporal.

Wavefront imaging was performed on sample AC2. Three wavefronts were recorded for this sample for three orthogonal directions. The sample was sealed with tape. Rubber sealant was applied to tape seams to prevent water from invading the sample. The sealed sample was placed in a water-filled tank to ensure the same coupling between the transducers and locations on the sample. The receiver scanned a 60 mm by 60 mm region in 1.0 mm increments recording a 100-microsecond window of the waveform at each position.

2.4 Seismic Array

Two seismic arrays were used to send and receive compressional and shear waves through sample AC5. The B-array was composed of source and receiver plates each with four compressional-mode (Figure 3 labeled as P) and three shear-mode contact piezoelectric transducers (Figure 3 labeled as S). The C-array was composed of source and receiver plates each with five compressional-mode and four shear-mode contact piezoelectric transducers. All transducers had a central frequency of 1 MHz. The source and receiver plates for each array had transducer layouts that are mirror images of each other. The C-array plates were in contact with the top of the sample and the B-array plates were in contact with two opposing sides of the sample (Figure 3). The other

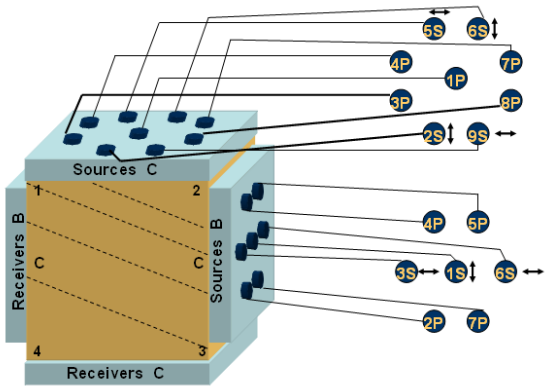

Figure 3. Seismic Array Setup. Plate C set contains nine sources (top plate) and nine receivers (bottom plate). Plate B set contains seven sources (right plate) and seven receivers (left plate). Arrows next to the shear transducers represent the direction of shear wave polarization.

two sides contained the inlet and outlet ports and no seismic data were recorded along that direction.

Seismic measurements were made on sample AC5 under different stresses and during fluid invasion with water. A 60-microsecond window of the transmitted signal was recorded for all source-receiver combinations for both the B-array and the C-array. During the fluid invasion experiment, both arrays were sampled every 2 minutes for the first 2.37 hours and then every 4 minutes for 9.73 hours.

3. RESULTS AND DISCUSSION

3.1 Wavefront Imaging Data

Wavefront imaging enables direct visualization of the isotropy or anisotropy in a sample. From our measurements on sample AC2, we observed anisotropic wavefronts caused by the fabric-controlled layering in the rock. Figure 4 contains a sketch of the observed layering in sample AC2 as observed from sides C, D and E. Also shown in Figure 4(c-e) are the arriving compressional wavefronts for waves propagated from sides A-to-C, sides B-to-D and sides E-to-F at three selected arrival times for sample AC2. The arrival times for the 3 sets of frames correspond to the first peak, first valley and second peak of the waves as shown in Figure 4b. In Figure 4b, the waves have been offset vertically for comparison.

If a sample is isotropic or nearly isotropic, the wavefront would be spherical and appear as a circle in two dimensions. However as shown in Figures 4c-e, the wavefronts are elliptical indicating anisotropy. By comparing the sketch of the layering in AC2 (Figure 4) to the wavefronts in Figure 4c-e, the wavefront propagated from side B-to-D is expected to exhibit the least anisotropy from the layers. From detailed acoustic maps, waves transmitted from side B-to-D exhibited the least variation in velocity (8%). Waves transmitted from sides A-to-C and from sides F-to-E exhibited 11% and 16% variation in velocity, respectively. In these two directions (A-to-C, F-to-E), layering in the rock is observed.

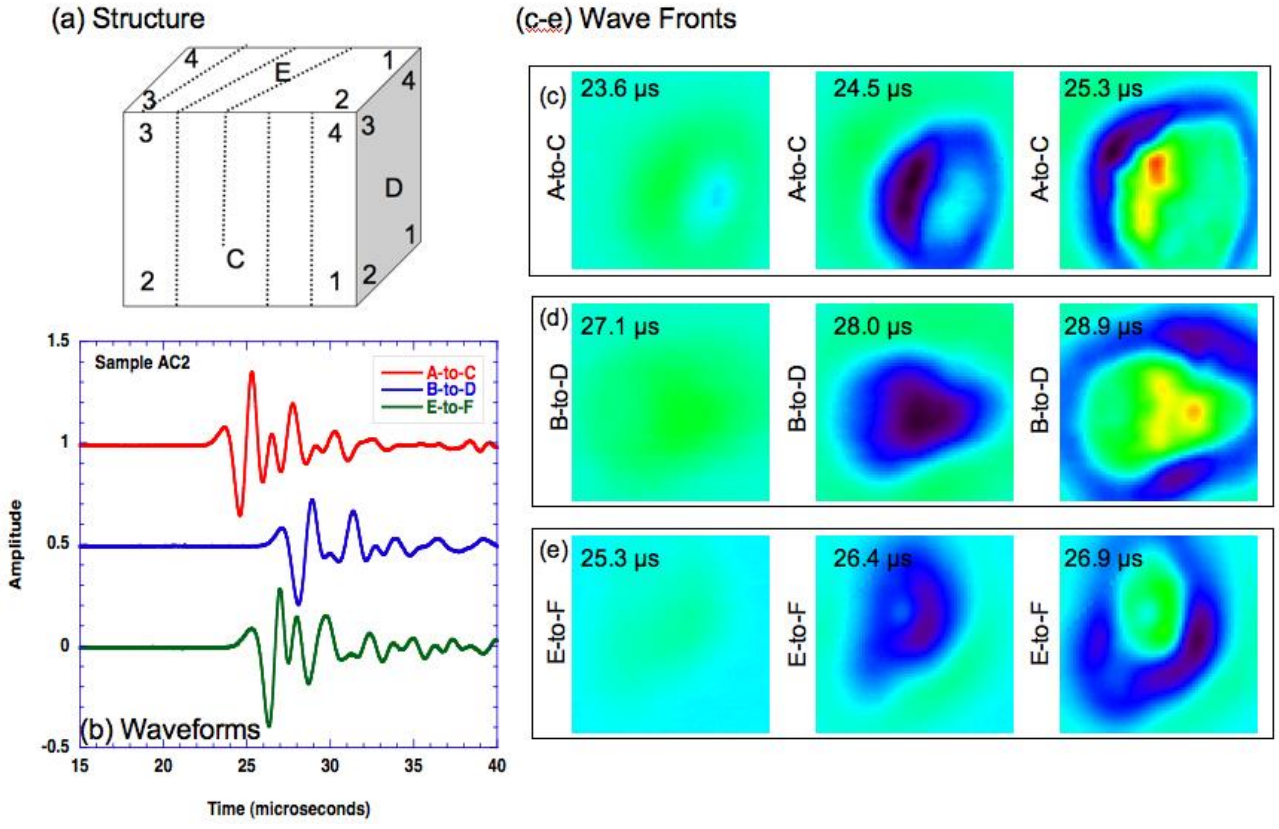

Figure 4. (a) Sketch of sample AC2 showing the orientation of the layering (dashed lines). (b) Transmitted compressional wave taken from the center of the wave front. Wavefronts for sides (c) A-to-C, (d) B-to-D, and (e) E-to-F are shown at selected arrival times listed in the upper left hand corner of each frame.

For side E-to-F, the seismic waves were propagated almost parallel to the layer and exhibited the most variation in velocity. This indicates that the fabric-induced structure in sample AC2 generates strong anisotropy and can cause strong energy confinement such as wave guiding or multiple internal reflections.

3.2 Seismic Array Data

Experimental measurements of compressional and shear waves were made for sample AC5 in the dry condition subjected to stresses of 1.3 MPa, 2.5 MPa, 3.8 MPa and 5.0 MPa. The compressional and shear waves propagated through AC5 exhibited only a slight sensitivity to stress for most source-receiver combinations. For example, the transmitted shear wave (1S-1S Array B) in Figure 5a shows a slight decrease in amplitude as stress increased and shows no significant change in arrival time. For the transmitted compressional wave (Figure 5b 2P-2P Array B), the amplitude of the wave increased slightly with increasing stress but was only a small delayed was observed. The small changes in arrival times are not systematic effects because no change in velocity with stress was observed on an aluminum standard with the same dimensions, for the same transducer configuration and for the same applied stresses. The very small changes in seismic velocities indicate that no significant increase or decrease in compressional and shear moduli occurs from micro cracks opening and/or closing under stress.

A water invasion experiment was performed on AC5 was for a stress of 1.3MPa. Significant changes were observed in both the compressional and shear waves (Figure 6). In Figure 6, the signals from the start of the invasion time=0 to 60 minutes into the invasion are shown. For source-receiver combinations 4P-4P Array C and 1S-1S Array B, as water was invaded into the sample the signal decreased in amplitude and was delayed.

For example, in Figure 6a, 30 minutes after fluid invasion the compressional wave amplitude decreased by 68% and the signal was delayed by 0.45microseconds. The arrival time of each signal was picked by hand directly from the graph. After 60 minutes, the amplitude decreased 80% relative to the initial dry condition (0 minutes) and was delayed 0.74 microseconds. In addition, the frequency content of the signal shifted to lower frequency as can be observed in Figure 6a by comparing the period of one cycle. Similar changes in amplitude, frequency content and signal delay are observed for the shear waves shown in Figure 6b. Based on the x-ray tomographic data (Figure 1) and from thin sections of the

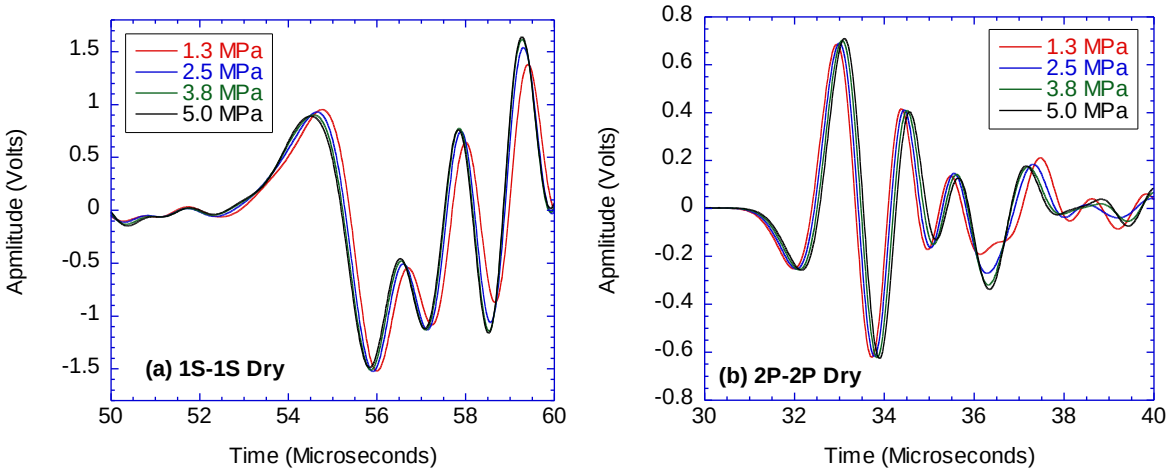

Figure 5. From the Array B: (a) Shear wave transmitted from 1S to 1S and (b) compressional wave transmitted from 2P to 2P for intact sample AC5 in the dry condition subjected to stresses of 1.3 MPa, 2.5 MPa, 3.8 MPa, and 5.0 MPa

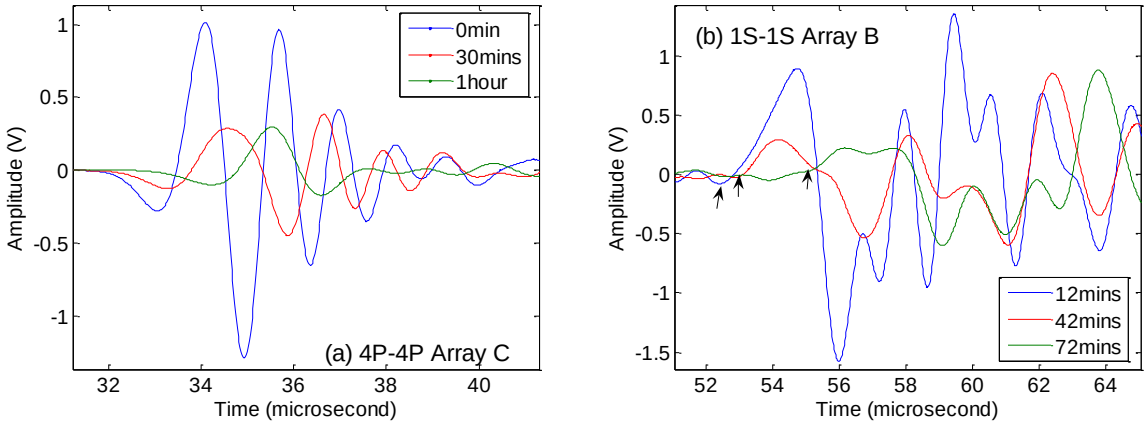

Figure 6. (a) Compressional waves recorded by Array C for transducer pair 4P-4P and (b) shear waves recorded by Array B for transducer pair 1S-1S. Signal shown are for 12 minutes, 42 minutes and 72 minutes after the initial invasion of water. Arrows on the signals in (b) indicate the shear arrival time from left to right for the blue, red and green.

sample (Figure 2), the layering in the sample varies in porosity, cement and density. The non-uniformity in these properties can lead to non-uniformity in the saturation of the sample. Patchy saturation induces heterogeneity in the seismic response of a sample and can behave like scatters that result in seismic wave attenuation particularly for high frequency components of the signal.

3.3 Fluid Front Mapping

We have shown in Figure 6 that water affected the amplitude of seismic waves propagated through these carbonate samples. As water invaded the sample, the amplitudes of the signals were observed to decrease with increasing water saturation. We used the data from the seismic array to track the invading fluid front to determine the dominant flow direction in the samples. The front was assumed to be between a source-receiver pair when the signal amplitude decreased by 50% over the initial value (i.e., dry condition). This assumption is based on a Fresnel diffraction study of an invading fluid in a fracture by Pyrak-Nolte et al. (2006). In their paper, they showed that when an invading fluid front is near the source-receiver line, seismic diffraction from the tip of the waterfront generated constructive interference and therefore increased transmission. As the water-air front advanced along the fracture, the transmission rapidly decreased when the front passed the source-receiver line and then reached a constant value. When the transmission dropped to one half of the initial value, the water front was shown theoretically to be directly between the source-receiver pair.

Figure 7 shows the positions of transducers (for details on the transducers distribution, see Figure 3 where the orientation of the rock is the same as that in Figure 7), and the water inlets relative to the layering in sample AC5. The effect of the fluid front on peak to peak amplitude and arrival time are shown in Figure 8 and Figure 9 for sample AC5 as a function of fluid invasion time. Figure 8 contains the results of the invading fluid front analysis for data from Array B, while Figure 9 contains results from Array C. As water was invaded into the sample, a change in amplitude was observed. For Array B, most source-receiver pairs exhibited a decrease in amplitude with fluid invasion (Figure 8). However, source-receiver pairs 1S-1S and 6S-6S exhibited an increase in shear wave amplitude prior to decreasing with continued fluid invasion. This was also observed in the Array C data in Figure 9(b&c) for pairs 1P-1P, 5S-5S and 6S-6S. The observed increase in amplitude prior to the decrease in amplitude is caused by constructive interference from diffraction from the tip of the fluid front (air/water interface) prior to when the front was under the sensors. From our analysis, we can estimate the time at which the fluid front was between a given source-receiver pair. For array B (Figure 8(a)), the times that water front arrived at 5P-5P and 7P-7P pair are nearly the same. However, it took 1.23 hour for water to reach 2P-2P pair, and 1.73 hour to 4P-4P pair. Array C shows a similar phenomenon that water tended to flow toward the right side prior to being sensed on the left side of the sample (see Figure 9(a)). It took 1.83 hours to reach 8P-8P, 2.58 hours to reach 9S-9S while it took 2.13 hours to reach 3P-3P and 3.1 hours to reach 2S-2S.

Figures 8a and 9a give a sense of the effect of the weak layering within the sample on fluid distributions. The invading front did not spread out uniformly through the sample. The invading front arrives earlier down dip from the ports than up-dip. This is confirmed by the data shown in Figures 8a & 9a for both arrays. Based on the transducer distribution shown in Figure 3, source-receiver pairs 2P-2P and 7P-7P from B-array and source-receiver pairs 7P-7P and 8P-8P from C-array are down dip from the inlet ports.

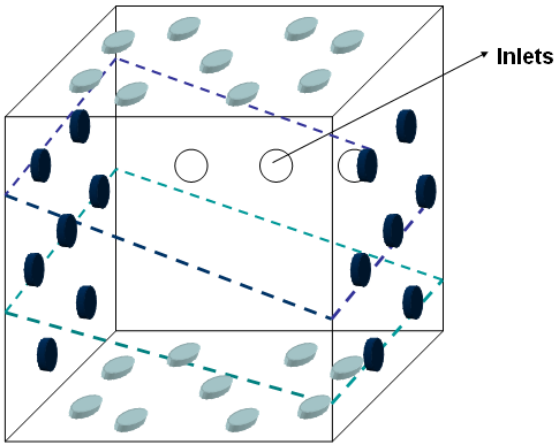

Figure 7. Layers are shown by dashed lines. Blue and dark blue small cylinders represent transducers on Plate C and Plate B respectively. White circles give the positions of the inlet ports on the backside of the sample. The outlet ports are not shown and mirrored the positions of inlets.

4. CONCLUSION

X-ray tomographic imaging data and thin section analysis showed that these carbonate samples contained fabric-controlled layering that exhibited variation in porosity among layers and within layers. From the wavefront imaging experiments, the density contrast between layers was sufficient to produce wave guiding and other internal reflections within the rock. The variation in density and porosity within these samples of Austin Chalk produced preferential flow paths along the layers. Our results demonstrate the complexity of flow paths and seismic response associated with layered systems, particularly weakly layered carbonate rock.

ACKNOWLEDGMENTS

The authors wish to acknowledge support of this work by the Geosciences Research Program, Office of Basic Energy Sciences US Department of Energy (DEFG02-97ER14785 08) and by ExxonMobil Upstream Research Company, as well as useful discussions with Shiyu Xu.

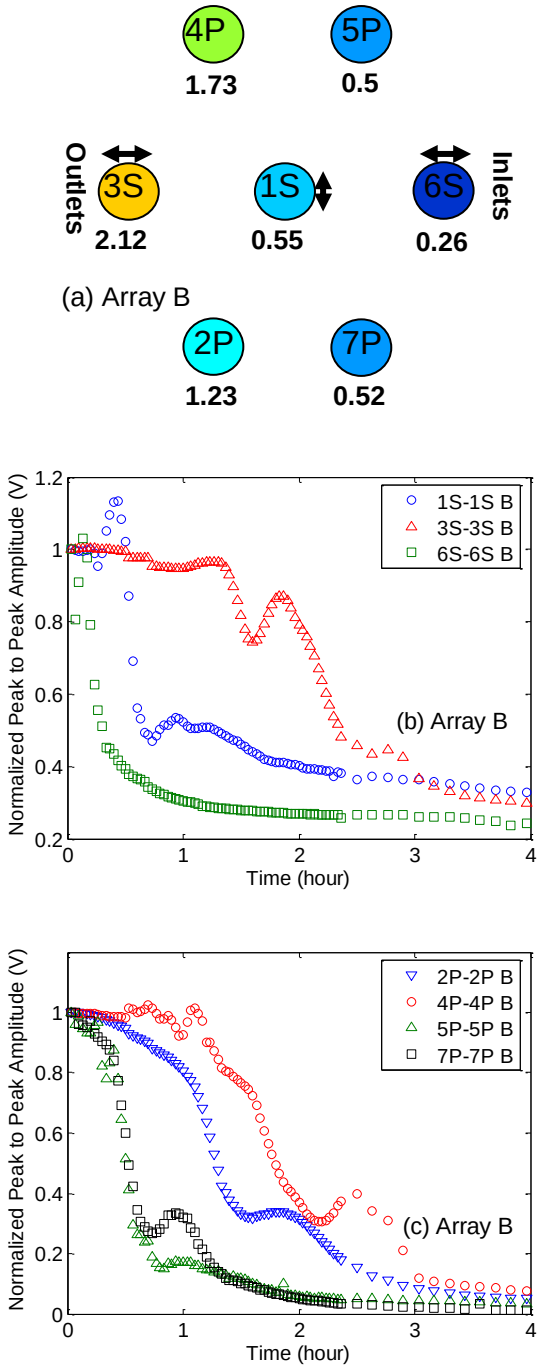

Figure8. Arrival time monitored by Array B and the corresponding peak-to-peak amplitude change of seismic wave. (a): Arrival time of fluid front interpreted from Array B data in hours. The fluid inlets are nearest 6S and the outlets are nearest to 3S. The color represents the time a transducer pair sensed water with blue to green to yellow representing increasing time. The arrows above the shear transducers represent the direction of polarization. (b): Peak-to-peak amplitude of shear waves as a function of invasion time for Array B source-receiver pairs 1S-1S, 3S-3S and 6S-6S. (c): Peak-to-peak amplitude of compressional waves as a function of invasion time for Array B source-receiver pairs 2P-2P, 4P-4P, 5P-5P and 7P-7P.

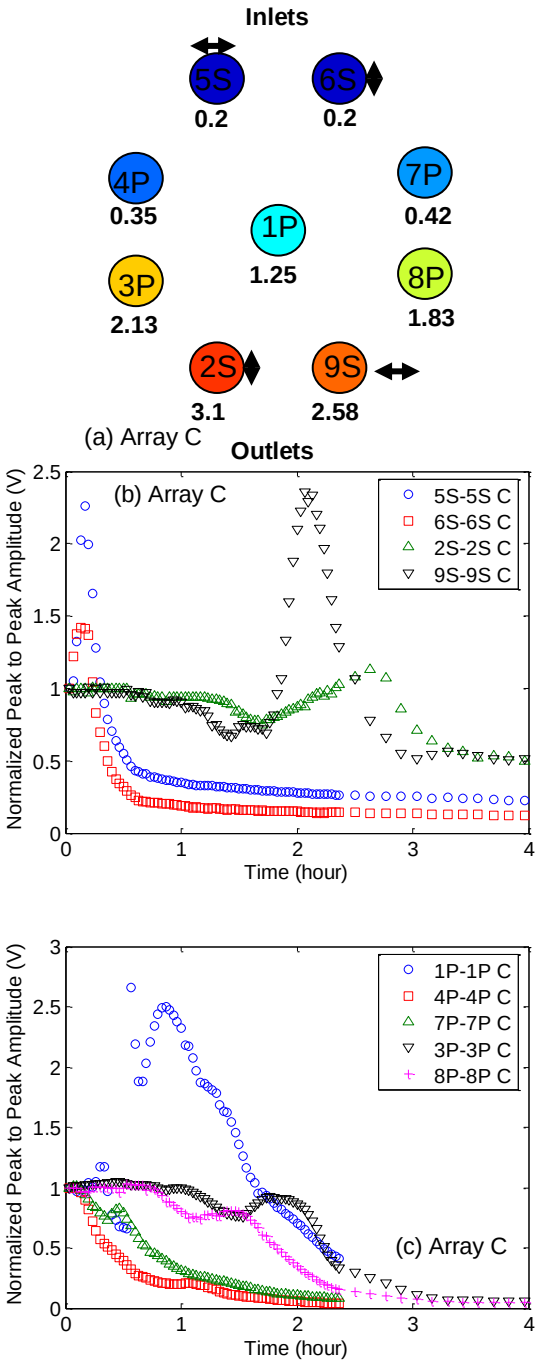

Figure 9. Arrival time monitored by Array C and the corresponding peak-to-peak amplitude change of seismic wave. (a): Arrival time of fluid front tested interpreted from Array C data in hours. The fluid inlets are nearest 5S & 6S and the outlets are nearest to 2S & 9S. The color represents the time a transducer pair sensed water with blue to green to yellow to red representing increasing time. The arrows above the shear transducers represent the direction of polarization. (b): Peak-to-peak amplitude of shear waves as a function of invasion time for Array C source-receiver pairs 2S-2S, 5S-5S, 6S-6S, and 9S-9S. (c): Peak-to-peak amplitude of compressional waves as a function of invasion time for Array C source-receiver pairs 3P-3P, 4P-4P, 7P-7P and 8P-8P.

REFERENCES

Durrast, H. and S. Siegesmund, Correlation between rock fabrics and physical properties of carbonate reservoir rocks, *International Journal Earth Sciences*, **88**, 392-408, 1999.

Mullenbach, B. L., Acoustic Imaging of Sediments. **1996** Master Thesis, University of Notre Dame: Notre Dame, Indiana. p. 140.

Nurmi, R., Charara, M., Waterhouse, M. and R. Park, Heterogeneities in carbonate reservoirs: *detection and analysis using borehole electrical imagery, Geological Society, London, Special Publications*, **48**, 95-111, doi:10.1144/GSL.SP.1990.048.01.09, 1990.

Oliger, A., Nolte, D. D. and L. J. Pyrak-Nolte, Focusing of seismic waves by a single fracture, *Geophysical Research Letters*, issue **5**, DOI/10.1029/2002GL016264, Citation Number 1203, 2003.

Pyrak-Nolte, L. J., Roy, S. and B. L. Mullenbach, Interface waves propagated along a fracture, *Journal of Applied Geophysics*, **35**, 79-87, 1996.

Pyrak-Nolte, L. J., Mullenbach, B. L., Li., X. and D. D. Nolte, Detecting sub-wavelength layers and interfaces in synthetic sediments using seismic wave transmission, *Geophysical Research Letters*, **26(1)**, 127-130, 1999.

Pyrak-Nolte, L. J, Nolte, D. D., de Pater, C. J. and J. Jocker **,** Monitoring Propagating Fracture Fronts: *Exploiting Fresnesl Seismic Precursors, Golden Rocks 2006, The 41st U.S. Symposium on Rock Mechanics (USRMS): "50 Years of Rock Mechanics - Landmarks and Future Challenges.*", Golden, Colorado, **June 17-21**, 2006.

Schoenberg, M. and F.K. Levin, Apparent attenuation due to interbed multiples, Geophysics, **39(3)**, 278-291, 1974.

Wolfe, J. P., Acoustic wavefronts in crystalline solids, *Physics Today*, **48(9)**, 34-40. 1995.

Xian, C., Nolte, D. D., and L. J. Pyrak-Nolte, Compressional waves guided between parallel fractures, *International Journal of Rock Mechanics & Mining Sciences*, **38**, 765-776, 2001